Thermodynamics and Molecular Dynamic Simulations of Three-phase Equilibrium in Argon (V6)

YAMADA, Yuri / 山田, 祐理 / 片岡, 洋右 / KATAOKA, Yosuke

(出版者 / Publisher)
法政大学情報メディア教育研究センター
(雑誌名 / Journal or Publication Title)
法政大学情報メディア教育研究センター研究報告
(巻 / Volume)
28
(開始ページ / Start Page)
1
(終了ページ / End Page)
15
(発行年 / Year)
2014
(URL)
https://doi.org/10.15002/00009839

Bulletin of Research Center for Computing and Multimedia Studies,
Hosei University, **28** (2014)

Thermodynamics and Molecular Dynamic Simulations of Three-phase Equilibrium in Argon (V6)

Yosuke KATAOKA [1)] and Yuri YAMADA [2)]

[1)] *Department of Chemical Science and Technology, Faculty of Bioscience and Applied Chemistry, Hosei University, 3-7-2 Kajino-cho, Koganei, Tokyo 184-8584, Japan, e-mail yosuke.kataoka.7t@stu.hosei.ac.jp*
[2)] *Department of Chemical Science and Technology, Faculty of Bioscience and Applied Chemistry, Hosei University, 3-7-2 Kajino-cho, Koganei, Tokyo 184-8584, Japan, e-mail bassoonist@mac.com*

SUMMARY

Very simplified equations of state (EOS) are proposed for a system involving argon and consisting of a perfect solid and a perfect liquid composed of single spherical molecules in which Lennard–Jones interactions are assumed. Molecular dynamics simulations of this system were performed to determine the temperature and density dependencies of the internal energy and pressure and the supercooled liquid state was also examined. The internal energy and pressure were found to be almost linear as functions of temperature at a fixed volume. The density dependencies of coefficients for pressure and the internal energy are written by linear functions of number density for simplicity and for ease of use.

KEY WORDS: equation of state, phase diagram, triple point, perfect solid, perfect liquid

1. INTRODUCTION

A three-phase equilibrium is typically observed in a Lennard–Jones (LJ) system [1] in which a perfect solid combined with a perfect liquid may serve as an idealized model. Various simplified equations of state (EOS) can be used to calculate the Gibbs energy of phase transitions between solid, liquid and gas phases based on such a model [2-7]. A more simplified EOS will be introduced in this work, applying the concept of the harmonic oscillator.

When using a harmonic oscillator approximation, the internal energy of the solid phase (U) is expressed by Equation (1).

$$U(V,T) = \frac{3}{2}NkT + U_{\mathrm{e}}(V, 0\ \mathrm{K}) + \frac{3}{2}NkT \tag{1}$$

Here, V is the volume of the system, T is the temperature, N is the number of spherical molecules and k is the Boltzmann constant. At low temperatures, the most important term in this equation is the average potential energy (U_e). The first term in Equation (1) represents the average kinetic energy while the last term is the average potential energy based on the harmonic oscillator approximation

When using this approximation, the pressure (p) of a solid may be expressed as the volume derivative of the average potential energy at the low temperature limit and the temperature effect may be expressed as a linear function of temperature as in Equation (2).

$$p(V,T) = \frac{NkT}{V} - \left(\frac{\partial U_{\mathrm{e}}(V, 0\ \mathrm{K})}{\partial V} \right)_T + \frac{6NkT}{V} \tag{2}$$

Received 8 March 2014
Published online 1 April 2014

The numerical coefficient of 6 in the last term of Equation (2) results from the FCC structure of solid argon [2]. The temperature dependent terms in Equation (2) and in the U_e term are valid only in the case of a harmonic FCC lattice. These equations may be generalized by applying suitable coefficients functions, *f(V)* and *g(V)*, which are obtained by fitting molecular dynamics (MD) [8] results as linear functions of temperature (Equations (3) and (4)).

$$U(V,T) = \frac{3}{2}NkT + U_e(V,0K) + g(V)NkT \tag{3}$$

$$p = \frac{NkT}{V} - \left(\frac{\partial U_e(V,0\ \mathrm{K})}{\partial V} \right)_T + f(V)NkT + \left(\frac{dg(V)}{dV} \right) NkT \ln(kT) \tag{4}$$

Here, *g(V)* and *f(V)* are functions of the volume obtained by the analysis of MD results, while the last term in Equation (4) is included to satisfy the thermodynamic equation of state [1]. These functions account for the effects of non-harmonic motion near the most stable portions of the solid structure. Over a wide density range, these functions represent interpolations between the condensed and gas phases and are also expected to serve a similar purpose in the liquid phase.

In this paper, the functions *f(V)* and *g(V)* will be very simplified as follows.

$$f(V) = \frac{6}{V}\frac{\sigma^3}{v}, v \equiv \frac{V}{N} \tag{5}$$

$$g(V) = \frac{3}{2}\frac{\sigma^3}{v} \tag{6}$$

Here, v is the volume per particle and the factor σ^3/v is the number density and it works as a weight function which accounts for dense regions of the argon. This factor also interpolates between the condensed and gas phases where the oscillator behavior vanishes.

Many studies have examined the EOS of Lennard–Jones systems [9~12]. Such studies are typically based on MD and Monte Carlo (MC) simulations of the equilibrium state [8] and the EOS thus obtained are used to investigate the gas–liquid equilibrium. Phase equilibria have been studied by both equilibrium and non-equilibrium molecular simulation techniques [11~22], both of which provide reasonably accurate results. The EOS results obtained in this work are also compared with these simulation results [11~22].

2. ANALYSIS OF MD SIMULATIONS

MD simulations [8] were performed in order to obtain the temperature and density dependencies of the internal energy and pressure. In this work, the molecular interactions of the spherical molecules were Lennard–Jones [1]. The Lennard–Jones potential (*u(r)*) may be expressed as a function of the interatomic distance (r) using the equation

$$u(r) = 4\varepsilon\left[\left(\frac{\sigma}{r} \right)^{12} - \left(\frac{\sigma}{r} \right)^{6} \right], \tag{7}$$

where ε is the depth of the potential well and σ is the separation at which $u(\sigma) = 0$. The constants ε and σ are in units of energy and length, respectively (Table 1).

Table 1. Lennard–Jones parameters [1]

(ε/k) / K	ε / 10^{-21} J	σ / 10^{-10} m	(ε/σ^3) / MPa	(ε/σ^3) / atm
111.84	1.54	3.623	32.5	320

NVT ensemble [8] simulations were performed at a number of fixed number densities (*N/V*) using a system with N = 256 and a sufficiently long cut-off distance (10^{-8} m) for calculations of potential energy and pressure, and Figs. 1 and 2 present examples of the results of these simulations. The average potential energy (U_e) and the pressure (p) of each phase were fitted by linear functions of the temperature (T) to give Equations (8) and (9).

$$\frac{U_e}{N\varepsilon} = a(U_e)\frac{kT}{\varepsilon} + \frac{U_e(V,0\ \mathrm{K})}{N\varepsilon} \tag{8}$$

$$\frac{p}{\varepsilon/\sigma^3} = a(p)\frac{kT}{\varepsilon} + \frac{p(0\ \mathrm{K})}{\varepsilon/\sigma^3} \tag{9}$$

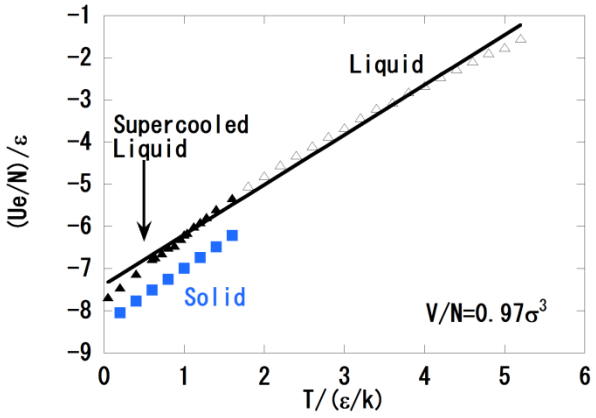

Fig.1 Average potential energy per particle U_e/N obtained from MD simulations at number density N/V = 0.97 σ^{-3} vs. temperature. The line of best fit for liquid phase data is shown.

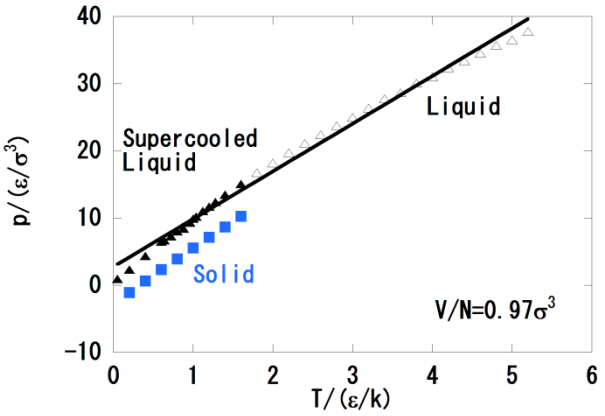

Fig. 2. Pressure obtained from MD simulations at number density N/V = 0.97 σ^{-3} vs. temperature. The line of best fit for liquid phase data is shown.

The average potential energy at 0 K, $U_e(V, 0\ \mathrm{K})$, is plotted in Fig. 3 and plots of the variations in the coefficients $a(U_e)$ *and* $a(p)$ are shown in Figs. 4 and 5. These coefficients may also be expressed as functions of *f(v) and g(v)* as in Equations (10) and (11).

$$a(U_e) = g(v) \tag{10}$$

$$a(p,\text{solid}) = 1 + f(v),\ \ a(p,\text{liquid}) = 1 + xf(v) \tag{11}$$

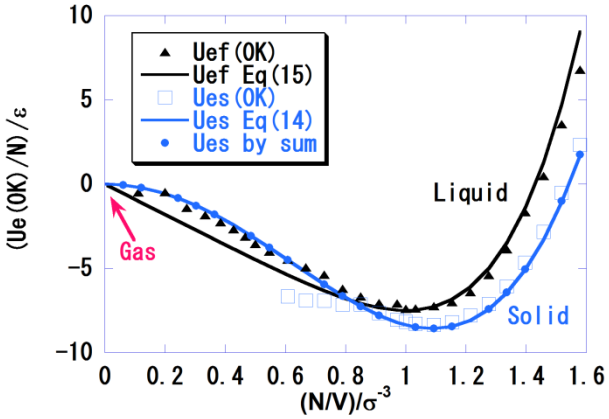

Fig. 3. Average potential energy per particle at the low temperature limit U_e(0 K)/N vs. number density N/V (See Equations (8) and (9)).

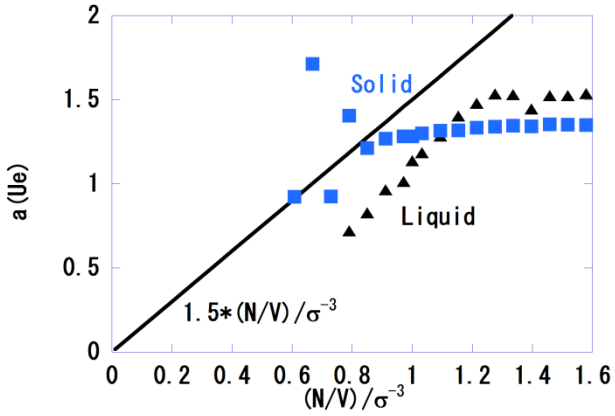

Fig. 4. Coefficient a(U_e) vs. number density N/V (see Equation (8)).

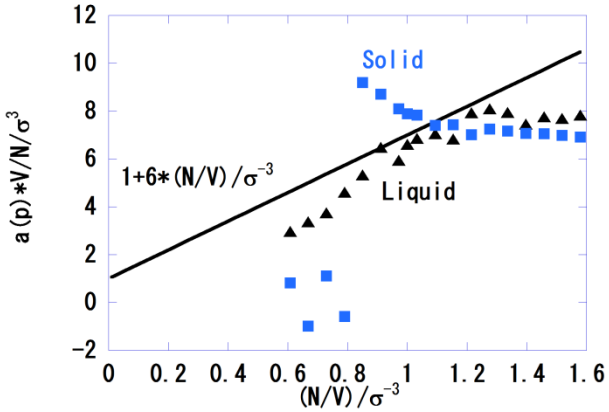

Fig. 5. The product of coefficient a(p) and volume per molecule V/N vs. number density N/V (see Equation (9)).

Here, *x* is an adjustable parameter which will be determined when fixing the triple point.

3. EQUATIONS OF STATE

The present EOS are as follows [6].

$$U(V,T) = \frac{3}{2}NkT + U_{\mathrm{e}}(V, 0\ \mathrm{K}) + g(v)NkT \tag{12}$$

$$p(V,T) = \frac{NkT}{V} - \frac{dU_{\mathrm{e}}(V, 0\ \mathrm{K})}{dV} + f(v)NkT + \left(\frac{dg(v)}{dv}\right)NkT\ln(kT) \tag{13}$$

$$\frac{U_{\mathrm{e,s}}(V, 0\ \mathrm{K})}{N\varepsilon} = 6\left(1+\frac{1}{128}\right)\frac{\sigma^{12}}{v^4} - 12\left(1+\frac{1}{5}\right)\frac{\sigma^6}{v^2},\ \text{(Solid)} \tag{14}$$

$$\frac{U_{\mathrm{e,f}}(V, 0\ \mathrm{K})}{N\varepsilon} = \left(1.5\frac{\sigma^{18}}{v^6} - 9\frac{\sigma^3}{v}\right),\ \text{(Liquid)} \tag{15}$$

$$g_{\mathrm{s}}(v) = g(v) = \frac{3}{2}\frac{\sigma^3}{v},\ f_{\mathrm{s}}(v) = f(v) = \frac{6}{V}\frac{\sigma^3}{v},\quad \text{(Solid)} \tag{16}$$

$$g_f(v) = g(v),\ \ f_f(v) = 0.886158 * f(v).\ \text{(Liquid)} \tag{17}$$

Here, the suffix *s* indicates the solid state while *f* refers to the fluid phase. It will be shown that there are both liquid and gas branches in the fluid EOS. In this study, the function $f_f(v)$ associated with the liquid state includes an adjustable parameter that is chosen, as in Equation (17), to reproduce the triple point and these EOS are considered as the EOS for a perfect solid and liquid. The last term in Equation (13) is included to ensure that Equations (12) and (13) satisfy the thermodynamic EOS [1].

The entropy change was calculated for a reversible isothermal expansion and a heating process at constant volume to the next change of state [1], as in Equation (18).

$$(V_i, T_i) \rightarrow (V_f, T_f) \tag{18}$$

This entropy change is expressed as follows in Equation (19).

$$\begin{aligned}
&\Delta S = \big(g(V_f) - g(V_i)\big)Nk + Nk\ln\left(\frac{V_f}{V_i}\right) + \big(F(V_f) - F(V_i)\big)Nk + \big(g(V_f) - g(V_i)\big)Nk\ln(kT_i) \\
&+\left(\frac{3}{2}Nk + g(V)Nk\right)\ln\left(\frac{T_f}{T_i}\right) \\
&F(v) = \int f(v)dv
\end{aligned} \tag{19}$$

Here the initial state is chosen as in the equations below.

$$T_i = \frac{\varepsilon}{k},\ \ V_i = Nv_{\max} \tag{20}$$

$$S_0 \equiv S_i = g(Nv_{\max})Nk + Nk\ln\left(Nv_{\max}\right) + F(Nv_{\max})Nk + \left(\frac{3}{2}Nk + g(Nv_{\max})Nk\right)\ln\left(\frac{\varepsilon}{k}\right) \tag{21}$$

Here the volume (v_{max}) is sufficiently large compared to the unit volume σ^3 and temperature is expressed in units of ε/k. Functions *F(V)* and *g(V)* are assumed to be zero in the initial state (see Equations (10), (11), (16) and (17)) and, as a result, the entropy change has the following form.

$$\Delta S(Nv,T) = \frac{3}{2}Nk\ln\left(\frac{kT}{\varepsilon}\right) + Nk\ln\left(\frac{v}{\sigma^3}\right) + F(v)Nk + g(v)Nk\ln\left(\frac{kT}{\varepsilon}\right) + g(v)Nk,$$
$$F(v) = \int f(v)dv \tag{22}$$

Hereafter, the entropy change from this S_0 is expressed simply as the entropy (S).

4. PHASE EQUILIBRIUM IN *T*–*P* SPACE

For a given value of temperature, T, the condition of the phase equilibrium between phases 1 and 2 in T–p space may be expressed by Equation (23).

$$p_1(V_1,T) = p_2(V_2,T),$$
$$\frac{G_1(V_1,T)}{N_1} = \frac{G_2(V_2,T)}{N_2}. \tag{23}$$

Since the EOS are known to be functions of volume and temperature, the above equation can be solved numerically [2, 3], and an example is shown in Figs. 6, 7 and 8 at the triple point.

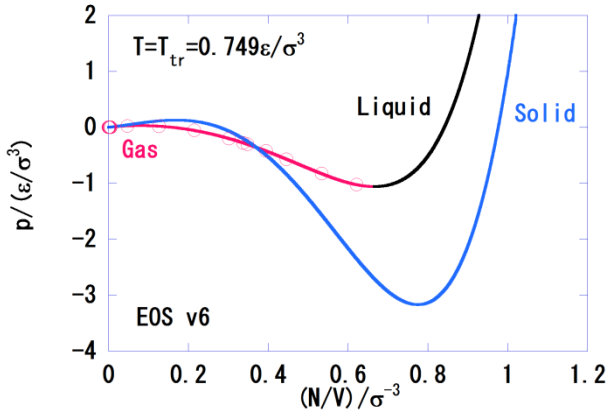

Fig. 6. Pressure vs. number density N/V at T_{tr} = 0.749ε/k.

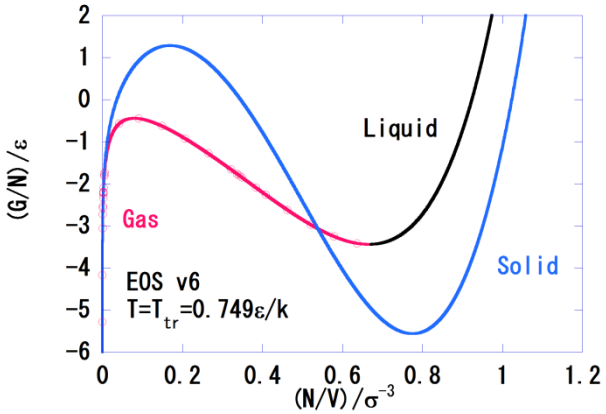

Fig. 7. Gibbs energy per molecule G/N vs. number density N/V at T_{tr} = 0.749ε/k.

Figure 6 demonstrates the density dependence of pressure. The Gibbs energy is plotted as a function of number density (N/V) in Fig. 7. As the pressure decreases, the liquid branch transitions to the gas branch within the van der Waals loop. The solid branch also changes to the gas branch, and has a slightly higher Gibbs energy than that of the previous gas branch originating from the liquid branch. The adjustable parameter in the liquid function $f_f(v)$ was chosen to reproduce the experimentally determined triple point of argon [23]. The thermodynamic

properties thus calculated are summarized and compared to both experimental and simulation results in Table 2, from which it is evident that the calculated properties are a reasonable approximation of the experimental and simulated data.

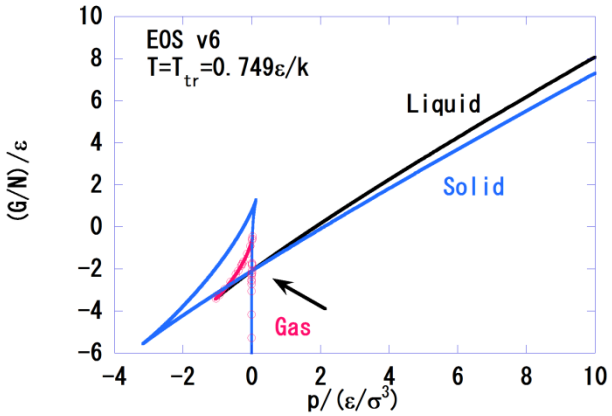

Fig. 8. Gibbs energy per molecule G/N vs. pressure at T_{tr} = 0.749ε/k. Arrow indicates the triple point.

Table 2. Comparison of EOS and experimental [23], MC [18] and MD [21] triple points. The mass density of the liquid (ρ_L) and the enthalpy change associated with the solid–liquid transition ($\Delta_{SL}H$) are also provided

	T_{tr}/K	P_{tr}/atm	ρ_L/(g/cm^3)	$\Delta_{SL}H$ (J/g)
EOS v1 [3]	69	1.75	1.129	60.5
EOS v2 [4]	84	0.3	1.134	29.8
EOS v3 [5]	77	0.31	1.181	28.6
EOS v4 [6]	84	1.3	1.158	27.4
EOS v5 [7]	84	0.68	1.179	26.4
EOS v6	84	0.8	1.176	24.2
exp [23]	84	0.68	1.417	28
MC [18]	77	0.32	1.182	26
MD [21]	74	0.58	1.205	24

The liquid–gas critical point was determined by numerically solving the following equation [1].

$$\left(\frac{\partial p}{\partial V}\right)_T = \left(\frac{\partial^2 p}{\partial V^2}\right)_T = 0 \tag{24}$$

Table 3 compares the critical points thus obtained with the experimental results [1] as well as the values determined by the molecular simulation method [17]. The calculated critical temperature is in good agreement with the experimental [1] and simulation results [17], with a relative error of 7%, while the EOS critical pressure is higher than that observed experimentally and the critical molar volume is close to the experimental result [1]. The comparison is satisfactory with respect to the critical constants.

The calculated transition pressure is plotted as a function of temperature in Fig. 9 and compared with the experimental [24–27] and simulation [13–22] results for argon. The pressure is plotted on a logarithmic scale due to its very wide range. The overall transition pressure for argon is well reproduced as a function of temperature. Figure 10 shows the transition temperature–number density relationship for argon and compares the calculated results with the simulation results [13–22]. The phase boundaries of the liquid and solid branches obtained from EOS calculations are close to the simulation results within the temperature range given by Equation (25).

$$0.5\frac{\varepsilon}{k} \le T \le 1.5\frac{\varepsilon}{k}. \tag{25}$$

The rather large deviations within the high temperature and high density regions results from the crude approximations in Equations (5) and (6). Some of the observed differences in the gas–liquid transition are also due to the estimated critical temperature.

Table 3. Comparison of EOS and experimental [1] and MD [15] critical constants of argon.

	T_c/K	p_c/atm	V_c/(cm^3/mol)
EOS v1 [3]	133	47	86
EOS v2 [4]	166	40	122
EOS v3 [5]	163	81	71
EOS v4 [6]	149	75	70
EOS v5 [7]	164	79	72
EOS v6	161	81	70
exp [1]	151	48	75
MD [17]	148	41	91
KN-EOS [10]	150	45	92

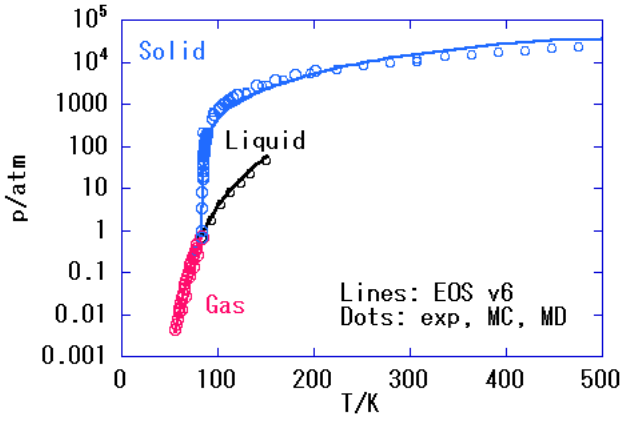

Fig. 9. Phase transition pressure vs. temperature for argon. Comparison of EOS, experimental [21–24] and simulation [13–21] results.

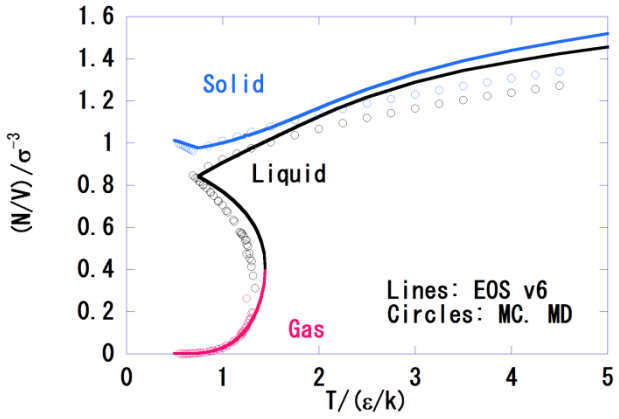

Fig. 10. Number density N/V vs. phase transition temperature for argon. Comparison of EOS and simulation results [13–21].

Figure 11 compares the calculated configurational entropy per molecule (S_c/N) with the simulation results [17]. The configurational entropy (S_c) has the following form in the perfect solid and liquid model.

$$S_c(V,T) = Nk\ln\left(\frac{V}{N\sigma^3}\right) + F(v)Nk + g(v)Nk\ln\left(\frac{kT}{\varepsilon}\right) + g(v)Nk + Nk \qquad (26)$$

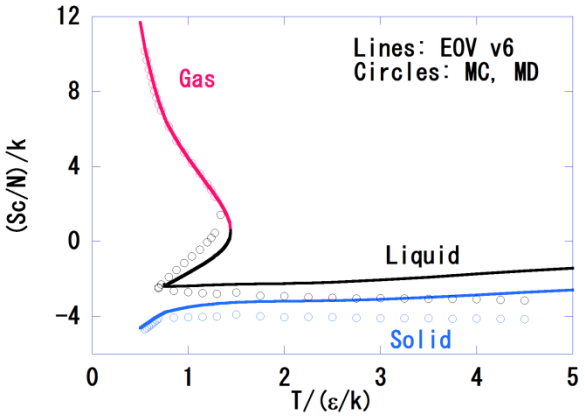

Fig. 11. Configurational entropy per molecule S_c/N vs. temperature in the phase equilibrium of argon. Comparison of EOS and simulation results [18].

The main feature of the phase equilibrium line in the solid–liquid transition is that the configurational entropies are almost constant as a function of temperature. This feature is reasonably well reproduced in our plot and therefore the overall features of the configurational entropy plot obtained using EOS are in agreement with the simulation results [18].

Figure 12 presents the average potential energy per molecule (U_e/N) at the phase boundaries, as shown in Equation (27).

$$\begin{aligned} U_{\mathrm{e,s}}(V,T) &= U_{\mathrm{e,s}}(V, 0\ \mathrm{K}) + g_{\mathrm{s}}(v)NkT, \ \text{(solid)} \\ U_{\mathrm{e,f}}(V,T) &= U_{\mathrm{e,f}}(V, 0\ \mathrm{K}) + g_{\mathrm{f}}(v)NkT. \ \text{(liquid)} \end{aligned} \tag{27}$$

These results are also compared with the simulation results [10, 18, 21]. The average potential energies of the solid, liquid and gas generally correspond well with the simulation results within the moderate temperature range defined by Equation (25). The reason why the average potential energies at liquid–solid equilibrium differ from the observed results in the region $T > 1.5\ \varepsilon/k$ is that the straight line $1.5\ \sigma^3/v$ deviates from the MD results in the high density region of Fig. 4. Figure 13 shows the configurational Helmholtz energy (A_c) as a function of the temperature along the solid–liquid phase boundaries. The calculated A_c value corresponds well with the MC simulation results [18] at low and intermediate temperatures.

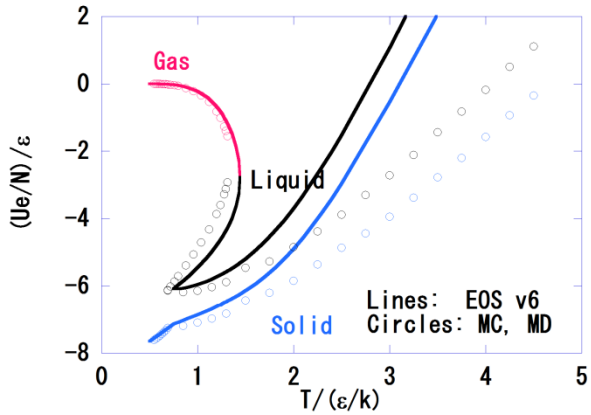

Fig. 12. Average potential energy per molecule U_e/N vs. temperature in the phase equilibrium of argon. Comparison of EOS and simulation results [18].

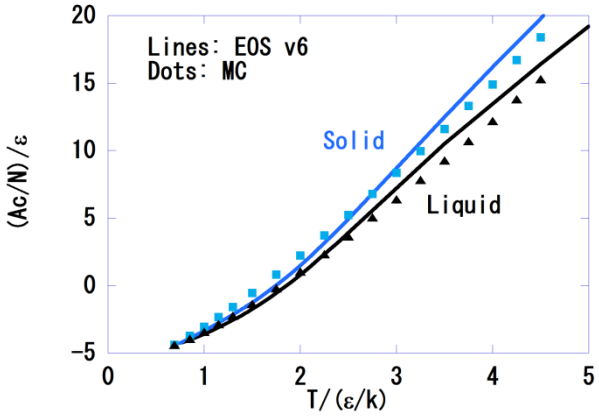

Fig. 13 Configurational Helmholtz energy per molecule A_c/N vs. temperature in the solid–liquid equilibrium of argon. Comparison of EOS and simulation results [18].

Finally, Fig. 14 compares A_c values at the solid–gas phase boundary with values obtained from MC simulations [18]. The EOS (v6) gives A_c values on the solid–gas phase boundary which are comparable with those of the MC simulation [18].

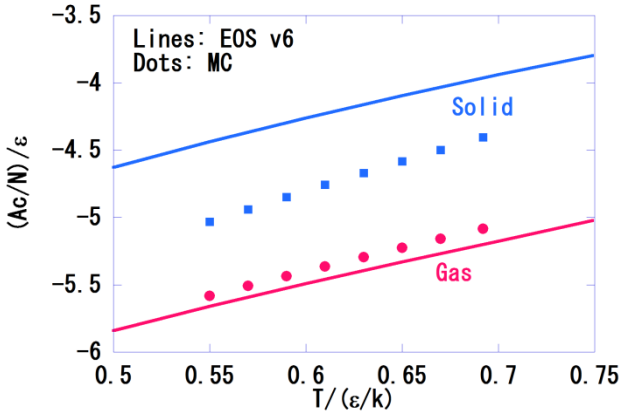

Fig. 14. Configurational Helmholtz energy per molecule A_c/N vs. temperature in the solid–gas equilibrium of argon. Comparison of EOS and simulation results [18].

5. THERMODYNAMIC PROPERTIES AT A CONSTANT PRESSURE

This section considers thermodynamic quantities at low pressures by comparing the EOS and simulation results. In Fig. 15, the calculated Gibbs energy values are plotted as a function of temperature at p = 1 atm = 3.13×10^{-3} ε/σ^3. These are compared with the Kolafa–Nezbeda (KN)-EOS data determined from many simulation results for the Lennard–Jones system [10]. When Fig. 15 is considered in detail near the transition points, the comparison is generally satisfactory. The entropies of the liquid and solid are negative due to the present choice of the entropy origin, and consequently the Gibbs energy plot differs from its usual form [1]. The melting point (T_m) and the boiling point (T_b) are fixed in Fig. 15 as in Equation (28).

$$\begin{aligned} T_m &= 83.8\ \mathrm{K} = 0.749\frac{\varepsilon}{k}, \\ T_b &= 85.9\ \mathrm{K} = 0.768\frac{\varepsilon}{k}, \\ p &= 1\ \mathrm{atm} = 0.313\times10^{-3}\varepsilon/\sigma^3 . \end{aligned} \tag{28}$$

These temperatures are close to the macroscopic experimental results [1].

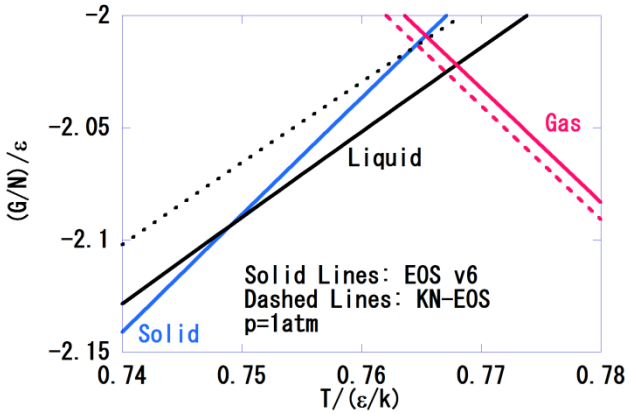

Fig. 15. Gibbs energy per molecule G/N vs. temperature at p = 1 atm. Comparison of EOS and simulation results [10]. The melting point is 0.749ε/k and the boiling point is 0.768ε/k.

Figure 16 shows the volume per molecule as a function of temperature at p = 1 atm. This is compared with the present MD results and the KN-EOS results [10]. The MD simulation was performed on an 864-particle system using a standard *NPT* ensemble [8]. This comparison demonstrates that the present simple EOS is applicable.

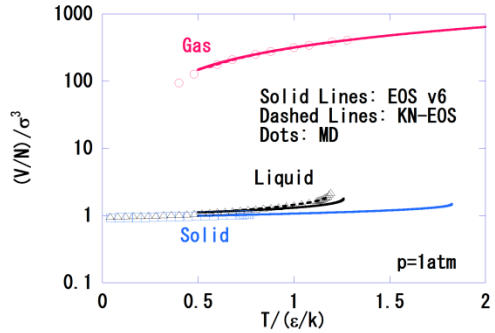

Fig. 16. Volume per molecule V/N vs. temperature at p = 1 atm. Comparison of EOS and simulation results [10], including the MD simulations of this study.

The internal energy is plotted as a function of temperature at p = 1 atm in Fig. 17, where the metastable state is also included. The stable liquid phase appears in the region

$$T_m \le T \le T_b . \tag{29}$$

For this reason, the comparison of the internal energy is satisfactory, as is also the case for the volume data.

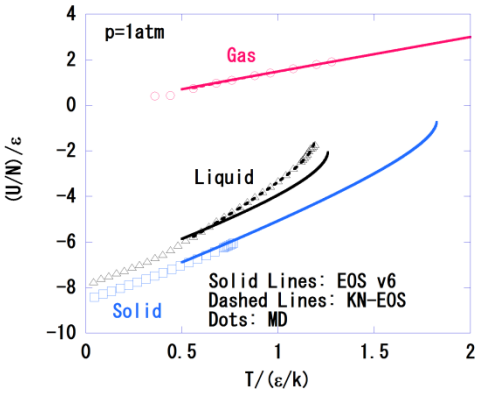

Fig. 17. Internal energy per molecule U/N vs. temperature at p = 1 atm. Comparison of EOS and simulation results [10], including the MD simulations of this study.

Figure 18 plots the enthalpy per molecule as a function of temperature at p = 1 atm. The calculated enthalpy is in agreement with the simulation results for the Lennard–Jones system, while the KN-EOS results are better than the present EOS in the liquid phase [10].

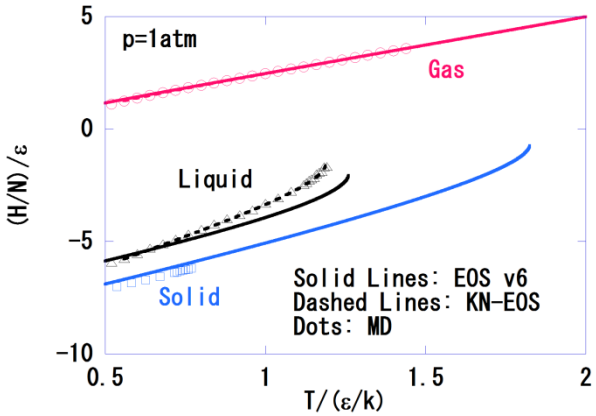

Fig. 18. Enthalpy per molecule H/N vs. temperature at p = 1 atm. Comparison of EOS and simulation results [10], including the MD simulations of this study.

The Helmholtz energy per molecule is shown in Fig. 19 and the entropy per molecule is depicted in Fig. 20. The overall features of the Helmholtz energy are satisfactory in comparison with the KN-EOS [10] while the entropy values for the liquid obtained by the EOS are close to those obtained from the simulations [10]. The entropies of the liquid and the solid are negative based on the present choice of the entropy origin.

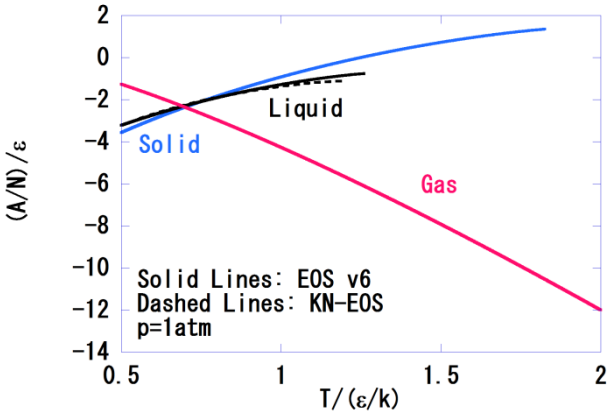

Fig. 19. Helmholtz energy per molecule A/N vs. temperature at p = 1 atm. Comparison of EOS and simulation results [10].

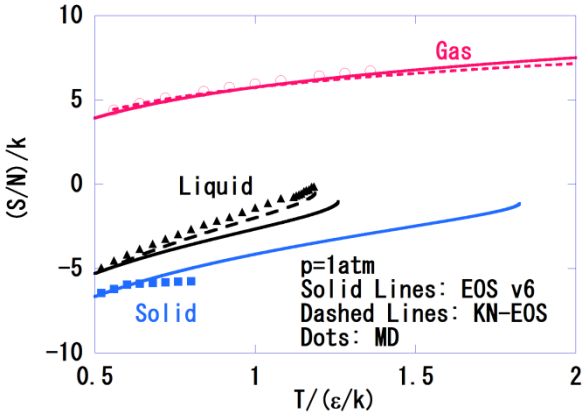

Fig. 20. Entropy per molecule S/N vs. temperature at p = 1 atm. Comparison of EOS and simulation results [10], including the MD simulations of this study. Entropy of the present MD result is calculated by the numerical integration of Cp/T and is adjusted with the EOS value at T = 0.5ε/k at each phase.

Figure 21 compares the expansion coefficient (α) calculated using the EOS with that obtained by simulations at p = 1 atm. Although the values of α for the liquid and solid differ slightly from those obtained by the simulations, the overall plots show reasonable similarity. The KN-EOS [10] gives a better expansion coefficient in the liquid phase than the present EOS.

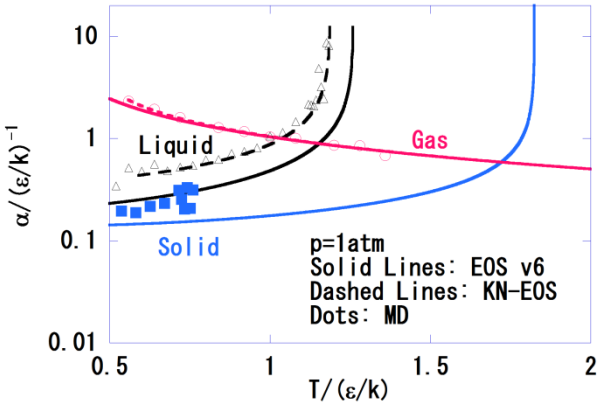

Fig. 21. Thermal expansion coefficient α vs. temperature at p = 1 atm. Comparison of EOS and simulation results [10], including the MD simulations of this study.

The isothermal compressibility (κ_T) at p = 1 atm obtained by the EOS is plotted in Fig. 22. Comparison of κ_T calculated by the EOS with the MD simulation results indicates that the present EOS satisfactorily explains differences in the order of magnitude of this term in each of the three phases.

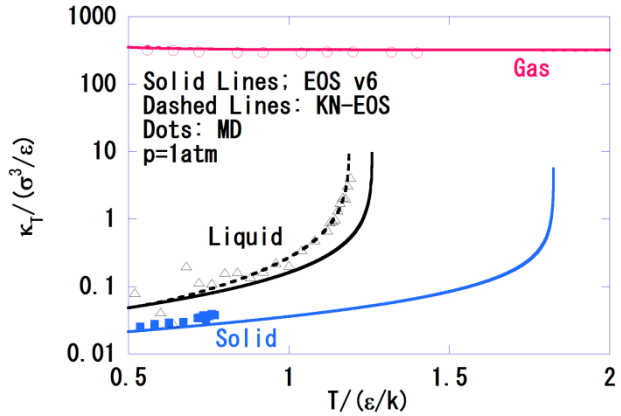

Fig. 22. Isothermal compressibility κ_T vs. temperature at p = 1 atm. Comparison of EOS and simulation results [10], including the solid phase MD simulations of this study.

Figure 23 shows the heat capacity under constant pressure (C_p) at p = 1 atm. The heat capacities in the gas and solid phases are in reasonable agreement with the results obtained by MD simulations. For C_p in the liquid phase, the calculated values are lower than those obtained by the MD simulation and the KN-EOS [10].

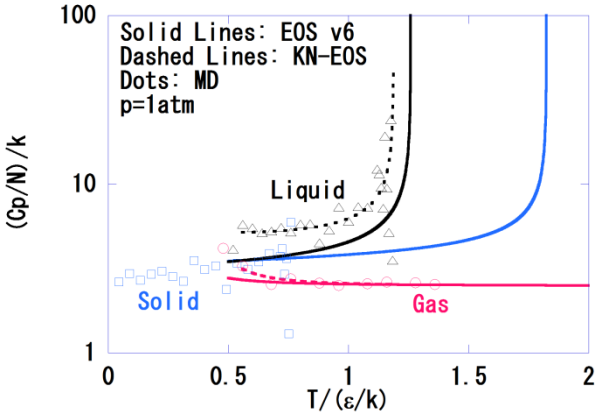

Fig. 23. Heat capacity at constant pressure per molecule C_p/N vs. temperature at p = 1 atm. Comparison of EOS and simulation results [10], including the MD simulations of this study.

6. THERMODYNAMIC CONSISTENCIES

The thermodynamic consistencies were examined using the following thermodynamic equation [1].

$$\left(C_p - C_V\right)\frac{1}{N} = \frac{\alpha^2 TV}{\kappa_T N} \tag{30}$$

The LHS and RHS of Equation (30) are shown in Fig. 24 for the three phases at p = 1 atm. No specific problems were encountered with the thermodynamic consistency.

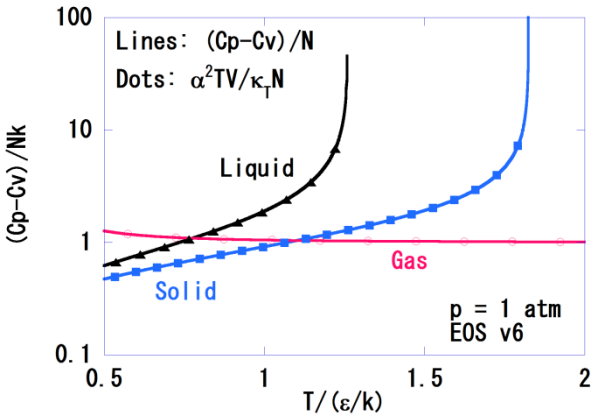

Fig. 24. Thermodynamic consistency test (see Equation (30)).

7. CONCLUSIONS

The phase transitions among the three phases of argon may be calculated with reasonable accuracy using our v6 EOS for a perfect solid and liquid, as represented by Equations (12)–(17), while the potential energy value of argon can be expressed using the Lennard–Jones pair potential. For this reason, the Lennard–Jones potential parameters, ε and σ, are not adjustable and thus only the coefficients in the functions of the EOS are adjustable parameters in the present EOS v6. The EOS for a perfect solid and liquid have a simple analytic form based on the harmonic oscillator approximation. We expect that this set of EOS may be employed for teaching thermodynamics in physical chemistry courses.

ACKNOWLEDGMENT

The authors would like to thank the Research Center for Computing and Multimedia Studies of Hosei University for the use of computer resources.

APPENDIX

An example of worksheet for calculation of Gibbs energy is shown as an attached file [28] (Table 4). Another worksheet to obtain volume for a given temperature and pressure is also given [29].

Table 4. Worksheets employed for phase transition calculations.

File name	Purpose	Example of figures
EOSv6_(T=1.00).xlsx	G/N vs. p plot	Figs. 3–14
EOSv6_(p=1atm).xlsm	solve $p(V,T_0)=p_0$	Figs. 15–24

REFFERENCES

[1] P. W. Atkins, *Physical Chemistry*, Oxford Univ. Press, Oxford (1998).
[2] Y. Kataoka and Y. Yamada, *J. Comput. Chem. Jpn.*, **10**, 98 (2011).
[3] Y. Kataoka and Y. Yamada, *J. Comput. Chem. Jpn.*, **11**, 81 (2012).
[4] Y. Kataoka and Y. Yamada, *J. Comput. Chem. Jpn.*, **11**, 165 (2012).
[5] Y. Kataoka and Y. Yamada, *J. Comput. Chem. Jpn.*, **11**, 174 (2012).
[6] Y. Kataoka and Y. Yamada, *J. Comput. Chem. Jpn.*, **12**, 101 (2013).
[7] Y. Kataoka and Y. Yamada, *J. Comput. Chem. Jpn.*, **12**, 181 (2013).
[8] M. P. Allen and D. J. Tildesley, *Computer Simulation of Liquids*, Clarendon Press, Oxford (1992).
[9] J. K. Johnson, J. A. Zollweg and K. E. Gubbins, *Mol. Phys.*, **78**, 591 (1993).
[10] J. Kolafa and I. Nezbeda, *Fluid Phase Equilib.*, **100**, 1 (1994).
[11] M. A. van der Hoef, *J. Chem. Phys.* **113**, 8142 (2000).
[12] M. A. van der Hoef, *J. Chem. Phys.*, **117**, 5092 (2002).
[13] J. -P. Hansen and L. Verlet, *Phys. Rev.*, **184**, 151 (1969).
[14] D. A. Kofke, *J. Chem. Phys.*, **98**, 4149 (1993).

[15] R. Agrawal and D. A. Kofke, *Mol. Phys.*, **85**, 43 (1995).
[16] H. Okumura and F. Yonezawa, *J. Chem. Phys.*, **113**, 9162 (2000).
[17] H. Okumura and F. Yonezawa, *J. Phys. Soc. Jpn.*, **70**, 1990 (2001).
[18] M. A. Barroso and A. L. Ferreira, *J. Chem. Phys.*, **116**, 7145 (2002).
[19] G. Grochola, *J. Chem. Phys.*, **120**, 2122 (2004).
[20] G. Grochola, *J. Chem. Phys.*, **122**, 046101 (2005).
[21] A. Ahmed and R. J. Sadus, *J. Chem. Phys.*, **131**, 174504 (2009).
[22] T. Kaneko, A. Mitsutake and K. Yasuoka, *J. Phys. Soc. Jpn*, **81**, SA012 (2012).
[23] *CRC Handbook of Chemistry and Physics*, Ed. D. R. Lide, CRC Press, Boca Raton (1995).
[24] K. Clusius and K. Weigand, *Z. Phys. Chem.*, **B46**, 1 (1940).
[25] *Kagaku-binran Kisohen*, The Chemical Society of Japan, Kaitei-yonhan, Maruzen, Tokyo (1993).
[26] R. K. Crawford and W. B. Daniels, *Phys. Rev. Lett.*, **21**, 367 (1968).
[27] W. van Witzenburg and J. C. Stryland, *Can. J. Phys.*, **46**, 811 (1968).
[28] EOSv6_(T=1.00).xlsx
[29] EOSv6_(p=1atm).xlsm

